

ADVANCED CONCEPTS FOR NUCLEAR EXPLOSION MONITORING APPLIED TO REGIONAL EVENTS IN THE ARCTIC REGION

Benjamin Kohl,¹ Hans Israelsson,¹ and Mark Fisk²

Science Applications International Corporation,¹ Mission Research Corporation²

Sponsored by Army Space and Missile Defense Command

Contract No. DASG60-03-C-0009

ABSTRACT

A number of innovative data processing algorithms and analysis techniques were developed to demonstrate improved capability for nuclear explosion monitoring. The focus was on techniques to address the challenges unique to the detection, location and characterization of events in the Arctic region using regional seismic array data. This research and development project was built upon the techniques and algorithms of others (e.g. as developed by NORSAR) and involved the development of new processing techniques and integration into a demonstration prototype system.

In support of the research and development activities, and as a test dataset to demonstrate improvements in capability, a comprehensive dataset of seismic recordings was assembled from historical regional events. The dataset included waveform segments from 40 different seismic stations recording historical nuclear and chemical explosions, earthquakes, and in-water explosions. In addition to the segmented datasets, 12 continuous days of waveform data, from key stations, were assembled into a fixed dataset that was used amongst other purposes, to assess noise characteristics and detection false alarm rates.

The above datasets were supplemented by theoretically scaling historical nuclear explosion waveform recordings down to levels allowing assessment of techniques applicable to low signal-to-noise ratios situations. The scaled waveforms were embedded in representative background noise and integrated into a database suitable for processing using both standard systems and new and improved algorithms. The embedded scaled events were used to conduct a detector fly-off experiment that systematically compared the performance of a new implementation of the adaptive beamforming (ABF) technique, the F-statistic detector, and a number of different recipes and configurations of the standard sta/lta detector running against conventional coherent and incoherent beams.

Detection comparison tests involving key regional seismic arrays (ARCES, SPITS) running against much broader and varied time windows, have the objective of better quantifying the performance of the ABF and F-stat detectors, and confirm that significant improvements in detection are achievable.

OBJECTIVES

Regional event detection, location and characterization have been areas of considerable interest and focus of nuclear explosion monitoring research and development for many years. This research and development project emphasized improved processing techniques. The scope of the project included signal detection of low SNR events, improved location particularly in the area of uncertainty error estimation and reference waveform utilization, and new techniques for event characterization.

RESEARCH ACCOMPLISHMENTS

In the following subsections we present many of the key results of the research. It should be noted that several key accomplishments were achieved and are summarized in bulleted form here, and are not described further in this paper.

- Developed a test and evaluation dataset of seismic recordings assembled from historical events recorded at the regional seismic arrays ARCES, FINES and SPITS
- Assembled 12 continuous days of waveform data from key stations into a fixed dataset
- Theoretically scaled historical nuclear explosion waveform recordings down to low SNR levels
- Developed a non-Gaussian error estimation and visualization tool
- Developed a scrolling-FK visualization tool to facilitate continuous review of array data in FK-space
- Applied phase-match filtering and spectral surface wave magnitude to enhance detection and reliable measurement of Ms for use with the Ms:mb discriminant.

The key research accomplishments are presented below.

Adaptive Beamforming and Detector Comparison Experiments

Noise at small regional arrays like ARCES is often partially coherent across the array and therefore not attenuated by conventional beamforming (CBF). At low frequencies (< 3Hz) coherent noise is often dominated by microseisms. Above 3 Hz, anthropogenic continuous narrow-band clutter is often from machinery and/or aircraft. Adaptive beamforming (ABF) updates a prediction error filter for each channel based on past noise to match the conventional beam directed at a specified slowness and azimuth. Consequently, ABF provides a distortionless response directed at the target beam while rejecting organized noise from other beams. ABF has the potential to remove coherent noise to reduce detection thresholds, increase bandwidth, increase signal-to-noise of weak onsets, and reduce false alarms.

ABF was tested against CBF using the prototype *Matlab* code to analyze noise windows (~1 hour) before and after small events recorded at ARCES and SPITS. Figure 1 compares the ABF and CBF Pn spectrograms recorded at ARCES. At the time, ARCES suffered from severe winter microseisms and anthropogenic clutter at several frequencies. Clutter from an aircraft is also seen. ABF attenuated microseisms below 3 Hz by 3-9 DB and narrow-band signals by 10-20 DB. A 3.1 Hz line associated to clutter was attenuated by ~30 DB.

ABF was coded in DFX (Detection and Feature eXtraction) and installed in a processing pipeline. The DFX installation of ABF is stable and adds only modest computational overhead compared to CBF. ABF output was configured for standard DFX STA/LTA detection. ABF was run for 24 hours on selected Pn and Sn beams optimized for signals at ARCES, NORES, FINES, and SPITS. Scaled explosion waveforms were embedded in the noise. STA/LTA detections from ABF and CBF output were compared. SNR were estimated from STA/LTA ratios of the embedded explosions.

The relative performance of four detectors was compared for one day, February 23, 2002. Scaled waveforms of a historical nuclear explosion were embedded in the data for three of the arrays, ARCES, FINES, and NORES. To assess detector performance at low SNRs, the waveforms were scaled and embedded at many different levels. The detector comparison or “fly-off” test included, as a baseline, the conventional detector with two different sets of recipes, one provided by NORSAR and employed in its operational processing (here labeled NORSAR) and another with a broad coverage of the Arctic region was composed for the test (labeled CBF below). The F-statistic detector

(FSTAT) was included in the “fly-off”, although this detector is often considered less effective at regional than at teleseismic distances.

The embedded explosions were detected by all four detectors - NORSAR, CBF, ABF, and FSTAT - down to the same lowest scaled magnitude. The top panel in Figure 2 compares the SNR of the detecting beams of the NORSAR and the ABF detectors with CBF as a reference. The average SNR is generally higher for the ABF detector than for the two conventional beam sets (NORSAR & CBF). The SNR of the FSTAT cannot be directly compared with those of the other detectors as its STA/LTA ratio is based on an F-statistic and not a signal beam.

Some of the detections could be associated with known events in the IDC REB and other bulletins. The ABF detector triggered on a clearly larger number of associated detections (REB data not available for NORES and SPITS association) than had other detectors. Unassociated detections are an indication of the false alarm rate. Unassociated detections vs. threshold vary among the detectors and from station to station, but the FSTAT detector generally had the smallest number of unassociated detections (bottom panel of Figure 2). The modest number of unassociated detections (per day) suggests that it is possible to lower the detection threshold in some instances by selective threshold tuning.

All detectors detected scaled explosions down to the same low-magnitude levels. The ABF provided higher SNR and association rates than the conventional detectors with similar unassociated detection rates. The FSTAT detector provided robust detection capability with the lowest unassociated rates among the detectors. Results suggest that using an F-statistic detector on the ABF output may provide both higher SNRs and lower false alarm rates. The “fly-off” test demonstrated the usefulness of scaled signals for detector assessment. The ABF and FSTAT show promise in lowering thresholds and lower false alarm rates and warrants further investigation.

Elevation Corrections and Data Resampling

The large elevation difference among elements of the SPITS array (0.140 km) compared with the horizontal aperture of the array (0.9 km) limits the performance of processing based on a horizontal planar array. Time delays used in beamforming only approximate actual time delays at array elements, resulting in reduced SNR and estimates of slowness and azimuth, based on FK analysis that may be biased.

To account for elevation differences and improve spatial coherence, 3D FK processing and beamforming were implemented in DFX. The vertical slowness for a given beam is defined from the horizontal slowness of the beam and the local P and S wave velocity at the array. A local average P velocity of 4.6 km/s for the SPITS array was estimated from teleseismic P waves recorded from about 100 broadly-distributed large events. The estimated value is in close agreement with estimates based on local data (Kremenetskaya et. al., 2001). The estimate was obtained by fitting values of horizontal slowness, azimuth, and vertical slowness of a plane wave across the array to pairs of time delays among array elements obtained from cross-correlation analysis.

Signals of small events recorded at the arrays SPITS and ARCES often contain significant energy above 10 Hz. Resampling of waveform data to a higher sampling rate further improves the alignment of element traces for the array beam. Improvements in SNR with resampling and elevation corrections are illustrated in Figure 3.

Elevation correction and data resampling of SPITS waveform data reduce bias in azimuth and slowness estimates. Elevation corrections and data resampling can also provide some SNR improvement. A consistent improvement was obtained for small events recorded at ARCES and SPITS. A 5 dB improvement was demonstrated for high frequency signals recorded at SPITS.

Phase Dependent Measurement Errors

In standard practice, location uncertainties are represented by the 90% coverage ellipse, which assumes that the data uncertainties are known *a priori* (IDC Doc. 5.2.1, 1998). If the *a priori* errors are independent and Gaussian, the confidence coefficient (or coverage parameter) follows a χ^2 -distribution with 2 degrees of freedom. The *a priori* errors are further divided into measurement and model errors, the former representing reading errors, the latter the uncertainties in the predicted travel-times. The actual coverage of the 90% error ellipse (i.e. the percent of true locations covered by the error ellipse 90% of the time) clearly depends on the reliability of the *a priori* error

estimates. Location calibration deals primarily with improved travel-time predictions and model errors. The primary focus of this study was the better estimation of measurement errors.

Currently, measurement errors are calculated from the signal-to-noise ratio (SNR) of the detection (Israelsson et. al., 1997). The linear relationship was derived from teleseismic P phases, but applied to all other phases. Therefore the measurement errors can be under-estimated for regional and secondary phases. While retaining the linear dependency on the SNR we have now derived coefficients for teleseismic and regional P, S, and Lg phases using REB readings for some 200 GT0-5 mining events and explosions in Fennoscandia and the Eastern European platform (Bondár et. al. 2002).

To test the phase-dependent measurement errors, we relocated the ground-truth events first using the current IDC error model, then the new measurement errors. In both cases IASPEI travel-time tables and model errors were applied. Finally, the events were located using the new measurement errors and path-dependent travel-time corrections with their corresponding model errors.

In conclusion, the enlarged phase-dependent measurement errors result in larger but more realistic error ellipses thus leading to significant improvements in coverage statistics. The actual coverage of the 90% error ellipse increased from 65% to 75%, when using the IASPEI velocity model, indicating that the IASPEI model errors are still underestimated. Phase-dependent measurement errors combined with calibrated travel-time predictions and model errors generate error ellipses close to 90% actual coverage.

Ground-Truth Through Use of Satellite Imagery and Terrain Elevation Data

In the development of the test and evaluation datasets, a number of published sources (Izdat, 2000, Richards, 2000 amongst others) were reviewed in order to select ground-truth events for testing and evaluating event location techniques. Given that there were inconsistencies between the published sources (e.g. the Oct. 24, 1990 nuclear explosion) and the importance of GT locations, we reexamined the waveform data for the historical nuclear explosions along with satellite imagery and terrain elevation data to assess GT attributions.

Standard imagery analysis techniques were applied to a series of 1m resolution commercial satellite images taken in 2000 to determine all known man-made features on the images, with a particular emphasis on identifying adits. Based on estimated yields, consequent overburden requirements and possible adit locations we were able to map out those portions of the test site that could realistically contain the largest of the nuclear explosions recorded since 1984. Figure 4 shows a map of the Matochkin Shar test site area, showing that the generally accepted location (Richards, 2000) for the Oct. 24, 1990 event appears to be slightly mislocated. A relocation of the event using a combined waveform cross-correlation, master event location technique also points to the event being about 1-2 km farther west than described by Richards, 2000.

Cepstral Analysis of Seismic Recordings of In-water Events

In-water explosions that do not breach the surface produce bubble pulses. In-water and shallow underground events can also produce water column reverberations. Both effects cause interference of the signals that are observed as modulations (or scalloping) in spectra and peaks in cepstra at corresponding delay times. Because these are near source effects, scalloping is generally present in all seismic phases at stations with adequate SNR over a sufficient bandwidth.

Spectral analysis is often advantageous in cases of limited bandwidth, which can obscure valid cepstral peaks and introduce false alarms. However, it is not clear how to quantify the significance of spectral scalloping. Thus, we use cepstral peak measurements because their significance can be quantified (Bonner et. al. 2000), and we apply a stringent significance level and physical constraints, based on local bathymetry and source yield, to eliminate spurious peaks.

The significance of a cepstral peak at a delay time, td , is quantified by defining $F_{2,2(N-1)}(td) = Nx(td)^2/var(td)$, where N is the number of cepstra computed for each seismic phase, $x(td)$ and $var(td)$ are the mean and variance of the cepstra at td . Under the hypothesis that the peak is zero, this quantity has an F-distribution with 2 and $2(N-1)$ degrees of freedom. This hypothesis is rejected if $F_{2,2(N-1)}(td)$ is greater than the percentile of the F-distribution at a

given significance level, which we set at 0.005. Figure 5 shows an example of this analysis for the main *Kursk* explosion on 12 August 2000.

Physical interpretation of cepstra is modeled by exponential time functions for the primary pressure wave and bubble pulses, convolved with ocean surface and bottom reflections for a given water depth, event depth, and yield (Baumgardt and Der, 1998). The cepstrum of this theoretical time function is computed and peaks in the model and data cepstra are compared to estimate the source depth and yield that provide the best fit (Figure 5). For the Kursk explosion, the estimated source depth and yield are approximately 104 meters and 5.5 tons, respectively.

Regional 3-C Pn/Sn Spectral Ratio Discriminant

Pn/Sn amplitude ratios are corrected for attenuation that is modeled by: $\log(\text{Pn/Sn}) = a + bD$, where D is the epicentral distance (in degrees), and the coefficients a and b are estimated by combining earthquake data from ARCES, KEV, and NORES. Estimated coefficients for Pn/Sn(6-8 Hz) are $a = -0.890$ and $b = 0.056$. Similar distance dependence is estimated using explosion data, supporting applicability of the attenuation corrections for both explosions and earthquakes.

Spatial variations of Pn/Sn are treated by kriging (Bottone et. al, 2002) station-averaged, distance-corrected $\log(\text{Pn/Sn})$ data for earthquakes, assuming a constant offset between explosions and earthquakes. Kriging station-averaged data, versus individual station data, provides slightly more robust corrections by reducing random variations. Kriging requires a correlation length and residual and calibration variances as input parameters. The residual variance is estimated from a cluster of 20 earthquakes near Steigen, Norway to be 0.108. The total variance of the station-averaged, distance-corrected $\log(\text{Pn/Sn})$ data for the regional earthquakes is 0.142. The difference of these variances yields an estimated calibration variance of 0.092. For kriging, the residual and calibration variances are set conservatively at 0.11. A correlation length of 5 degrees is used, typical of estimates in previous studies (Bottone et. al, 2002). The leave-one-out procedure is used to compute the corrected data values.

Figure 6 shows the correction and uncertainty grids and corrected data values. All of the markers for the explosions are black circles, corresponding to values above the local earthquake mean. The correction grid exhibits systematic spatial variations, which range from about -0.10 to +0.09. The grid of the posterior calibration standard deviation approaches the prior calibration standard deviation of 0.11 far from data, and is reduced to about 0.035 near the clusters of events in the Barents Sea south of Spitzbergen and near Steigen, Norway.

The Pn/Sn criteria treat the fact that each event has a different calibration uncertainty associated with the kriged corrections. Let R denote station-averaged, distance-corrected $\log(\text{Pn/Sn}(6-8 \text{ Hz}))$. An event is rejected as an earthquake if:

$$\frac{R - \bar{R}_{eq}(x_0)}{\sqrt{\sigma_{r,eq}^2 + \sigma_{c,eq}^2(x_0)}} > z_{\alpha},$$

where $\bar{R}_{eq}(x_0)$ is the posterior mean (kriged correction term) and the denominator includes the residual and posterior calibration variances, estimated at the location, x_0 , of the event being tested. Similarly, an event is rejected as an explosion if:

$$\frac{R - \bar{R}_{ex}(x_0) - \Delta}{\sqrt{\sigma_{r,ex}^2 + \sigma_{c,ex}^2(x_0)}} < -z_{\alpha},$$

where $\Delta = 0.64$ is the mean difference of $R - \bar{R}_{eq}(x_0)$ for explosions and earthquakes and $\sigma_{r,ex}$ is the residual standard deviation for explosions, estimated from nuclear explosion data to be 0.11. In the preceding criteria, z_{α} is the $(1-\alpha)$ -percentile of the standard normal distribution with zero mean and unit variance. For 0.005 significance level, $z_{\alpha} = 2.576$.

REFERENCES

Baumgardt, D. and Z. Der, "Identification of presumed underwater chemical explosions using land-based regional arrays," *Bull. Seism. Soc. Am.*, **88**, 581-595, 1998.

25th Seismic Research Review - Nuclear Explosion Monitoring: Building the Knowledge Base

- Bondár, I., K. McLaughlin, X. Yang, J. Bhattacharyya, “Assessing location improvements without ground truth data,” *Seism. Res. Let.*, **73**, 227, 2002.
- Bondár, I., S. Myers, R. Engdahl, E. Bergman, “Epicenter accuracy based on seismic network criteria”, submitted to *Geophys. J. Int.*, 2002.
- Bonner, J., D. Reiter, and B. Shumway, “Application of a Cepstral F-statistic for Improved Depth Estimation”, 22nd *Annual DoD/DOE Seismic Research Symposium Proceedings*, v. 2, 02-07, 2000.
- Bottone, S., M. Fisk and G. McCartor (2002). Regional seismic event characterization using a Bayesian formulation of simple kriging, *Bull. Seism. Soc. Am.*, **92**, 2277-2296.
- Engdahl, E.R., R. van der Hilst, R. Buland, “Global teleseismic earthquake relocation with improved travel times and procedures for depth determination,” *Bull. Seism. Soc. Am.*, **88**, 724-743, 1998.
- Grant, L., J. Coyne, and F. Ryall, “CSS Ground-Truth Database: Version 1 Handbook,” Center for Seismic Studies Technical Report, C93/05, 1993.
- Hanson, J., R. Bowman, and G. Beall, “An Advanced Concept Demonstration for Monitoring the Indian Ocean,” 24th *Annual DoD/DOE Seismic Research Review Proceedings*, 04-02, 2002.
- IDC Processing of Seismic, Hydroacoustic and Infrasonic Data, *IDC Documentation 5.2.1.*, 1998.
- Israelsson, H., G. Beall, H. Swanger, Independent modeling of time measurement and model errors, *Center for Monitoring Research*, CCB-PRO-97/24, 1997.
- Izdat, USSR Nuclear tests. Novaya Zemlya Test Site: Ensuring general and radiation safety (in Russian), Eds. N. P. Voloshin, G. E. Zolotukhin, G. A. Krasilov, V. A. Logachev, A. M. Matushenko, G. A. Mikhailikhina, A. K. Tchernyshev, and O. E. Shamov. Izdat publishing office, Moscow, 2000
- Kremenetskaya, E, S. Baranov, Y. Filatov, V.E. Asming, F. Ringdal, “Study of seismic activity near Barenetsburg mine,” in NORSAR Scientific Technical Report No.1-2001, Kjeller, July, 2001.
- Kremenetskaya, E., Private communication, April 2000.
- Mueller, R. A., and J. R. Murphy, “Seismic characteristics of underground nuclear detonations. Part I: Seismic Spectrum Scaling,” *Bull. Seism. Soc. Am.*, **61**, 1675-1692, 1971.
- Nicholson, T. M. Sambridge, O. Gudmundsson, “On entropy and clustering in earthquake hypocentre distribution,” *Geophys. J. Int.*, **142**, 37-51, 2000.
- NORSAR, Waveforms from selected events in the European Arctic, DE-AC04-99AL66001, 1999.
- Richards, P. G., Accurate estimates of the absolute location of underground nuclear tests at the northern Novaya Zemlya test Site, Second workshop in IMS location Calibration, Oslo, 2000
- Ringdal, F., and J. Fyen, “RMS Lg Analysis of Novaya Zemlya Explosion Recordings,” in NORSAR Semiannual Technical Summary, 1 October 90 – 31 March 1991, NORSAR Scientific Report 2-90/91, 53-67, 1991.
- Ringdal, F., Study of low-magnitude seismic events near the Novaya Zemlya nuclear test site, *Bull. Seismol. Soc. Am.*, **87**, 1563-1575, 1997.
- Stevens, J. L. and J. R. Murphy, “Yield Estimation from surface wave amplitudes,” *Pure and Applied Geophysics*, **158**, 2227-2251, 2001.
- Sultanov, D. D., J. R. Murphy, and Kh. D. Rubinstein, “A seismic source summary for Soviet peaceful nuclear explosions,” *Bull. Seism. Soc. Am.*, **89**, 640-647, 1999.

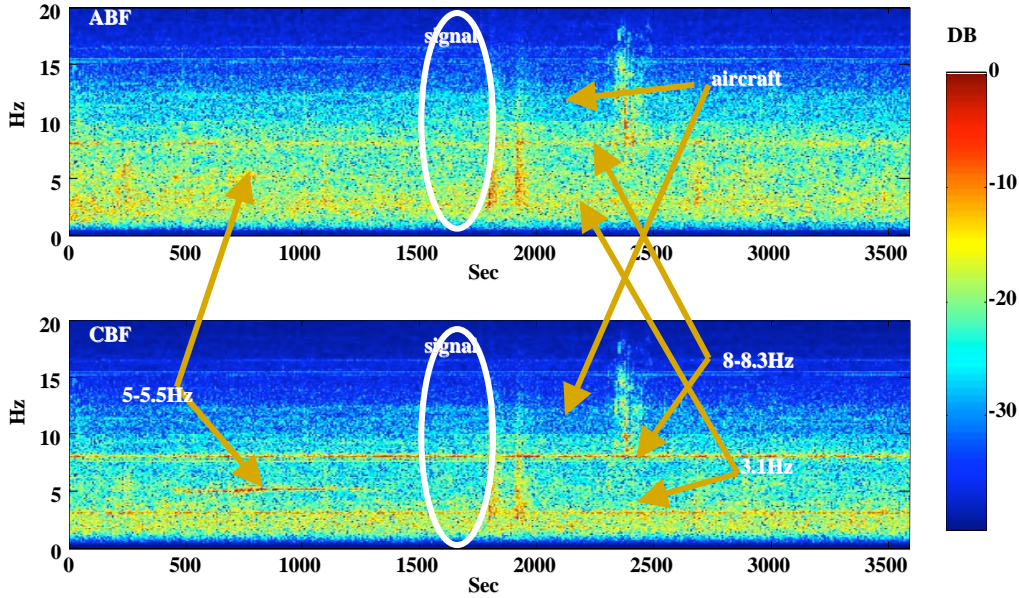


Figure 1: Pn beam ABF and CBF spectrograms for the 1996/01/13 event recorded at ARCES (DB w.r.t. max). Low frequency microseisms (<3 Hz), narrowband clutter (at 3.1, 5-5.5 and 8-8.3 Hz), and aircraft noise are attenuated, improving low frequency signal bandwidth and initial Pn arrival SNR.

SNR Ratio for Embedded Signals (dB)		
	NORSAR/CBF	ABF/CBF
ARCES	1.0+/-0.5	3.4+/-1.7
FINES	1.7+/-0.3	5.5+/-0.2
NORES	0.7+/-0.5	3.9+/-0.7

Unassociated ARCES

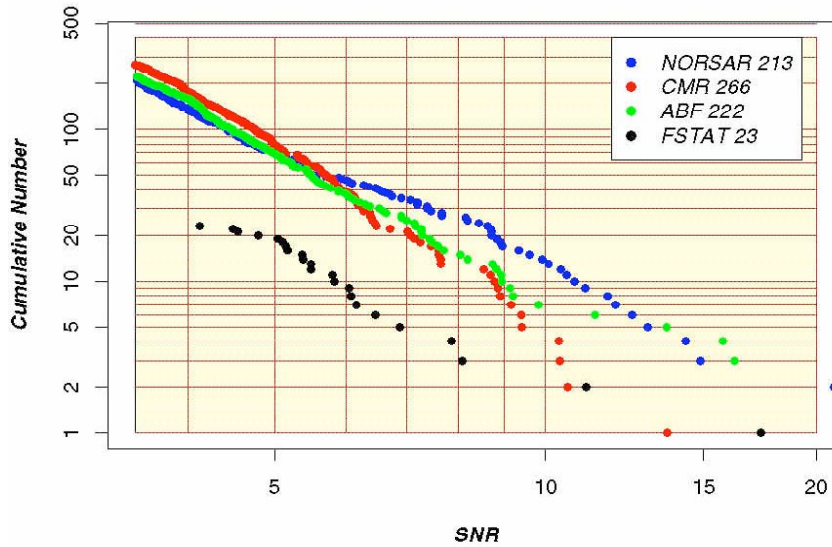


Figure 2: SNR and false alarm rate results of detector comparison experiment. The top panel shows relative SNR gain achieved by the ABF detector. The bottom panel shows the cumulative number of unassociated detections at the ARCES array versus SNR = STA/LTA ratio or Fstat. ABF and conventional beams show similar false alarms per day.

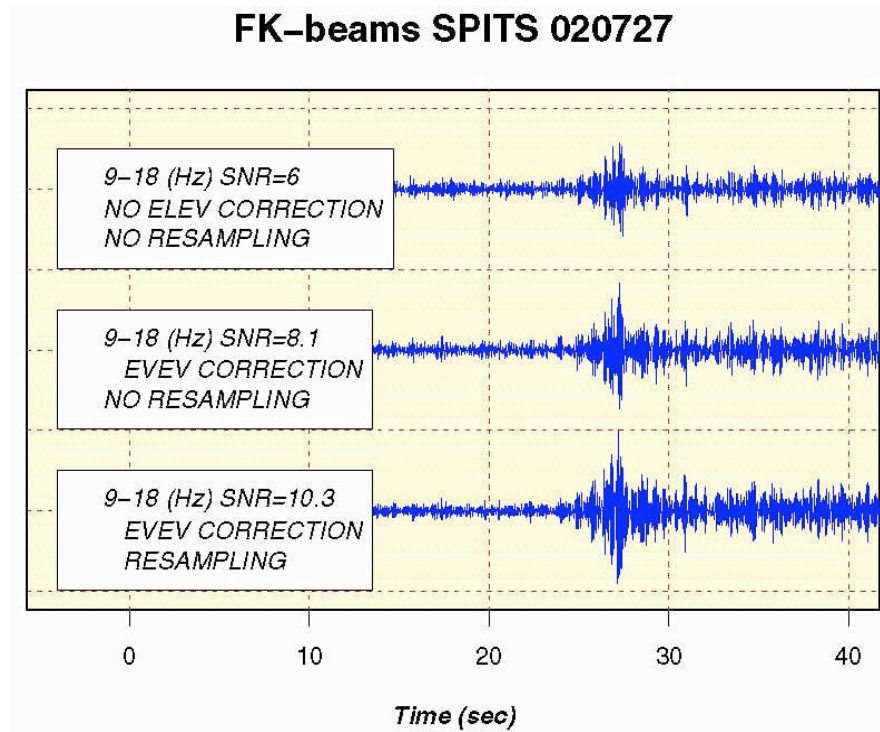


Figure 3: SNR of FK-beams improve by almost a factor of 2 at SPITS as a result of elevation corrections and resampling for small magnitude event (July 27, 2002).

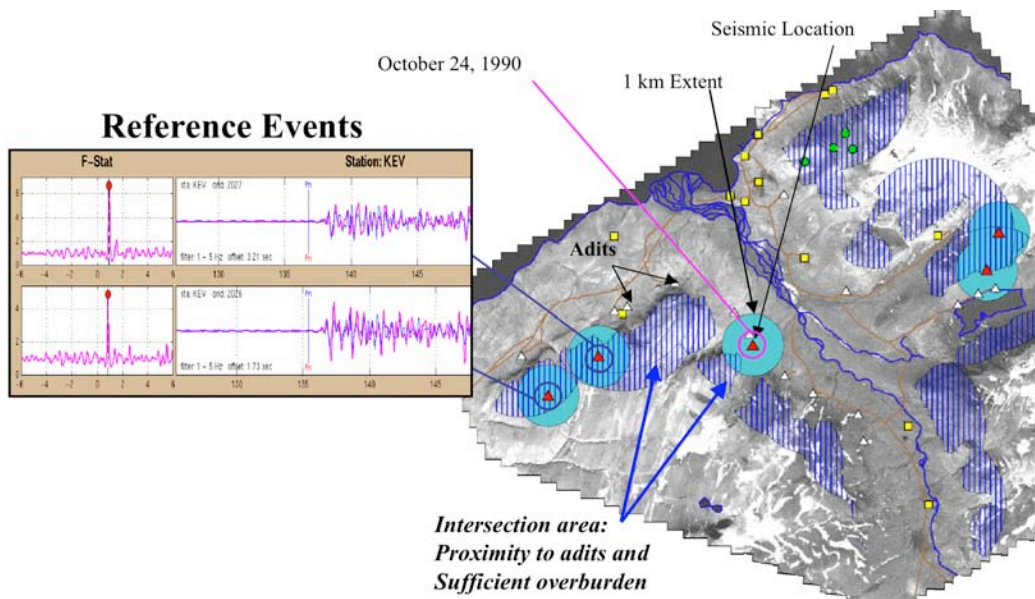


Figure 4: Map of the Matochkin Shar test site area showing visible adits (white triangles), other man-made artifacts (yellow squares) and seismic locations (red triangles) for the five largest nuclear explosions since 1984. The hatched area represents all those areas with at least 200 meter overburden and within 2 km of an adit, or with 3 km of any other visible man-made artifact. The fact that the seismic location of the Oct. 24, 1990 event falls outside the hatched area brings into question the designation of this event as GT1.

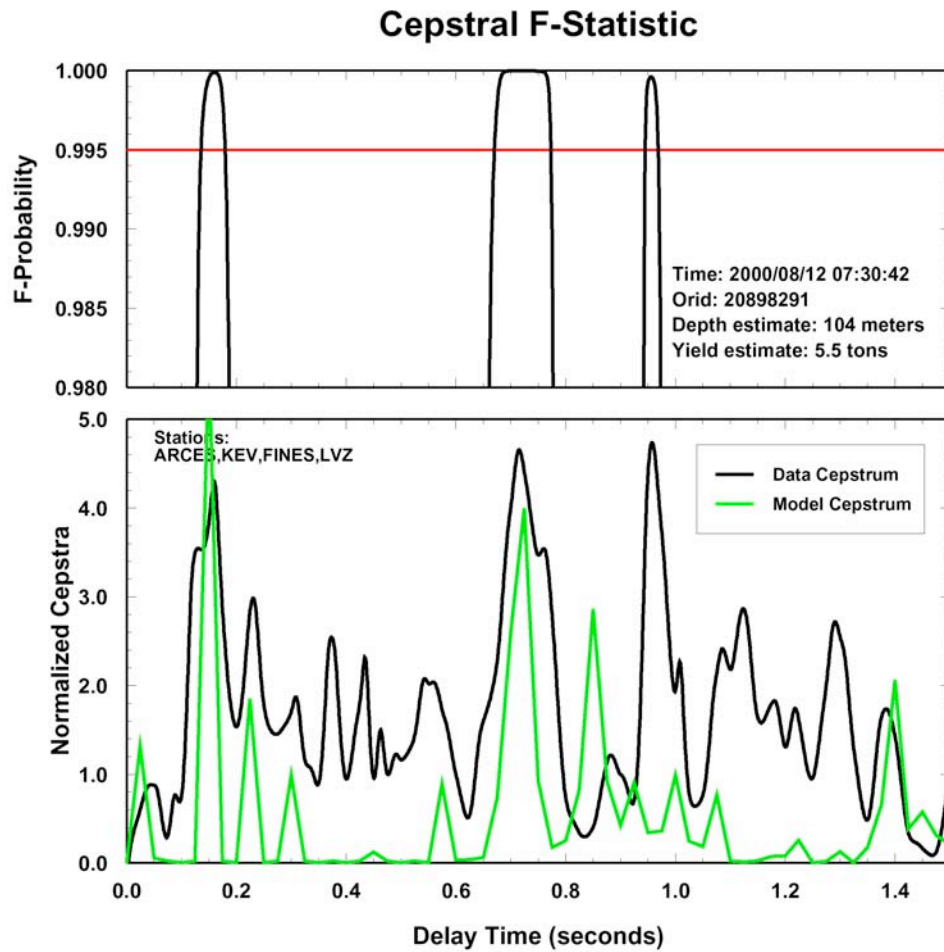


Figure 5: The lower frame shows the combined data cepstrum, using cepstra of regional phases at ARCES, KEV, FINES and LVZ for the August 12, 2000 Kursk explosion (black curve) and model cepstrum (green curve) that fits the main peaks of the data cepstrum. The upper frame shows the F-probability trace and threshold at a 0.005 significance level.

